10. EVOLUTION OF INSTRUMENT PARAMETERS

The geometrical instrument parameters describe the transformation from ideal, angular coordinates in the fields of view to the observable 'grid coordinates' connected with the slit pattern on the main grid. The instrument parameters were determined as part of the great-circle reductions, and while they are not of any direct astronomical interest, they are highly relevant for understanding the behaviour of the Hipparcos instrument. The transformation models used by the FAST and NDAC consortia are specified in this chapter and the resulting instrument parameters are shown as functions of time.

10.1. Introduction

The purpose of the great-circle reductions (Chapter 9) was to compute the coordinates of stars along designated reference great circles, the so-called star abscissae. In doing so, the geometrical distortions of the Hipparcos main field of view had to be determined as part of the least-squares solutions for the star coordinates. These distortions are described by the geometrical instrument parameters. While not of any direct astronomical interest, the instrument parameters and their temporal evolution are highly relevant for understanding the Hipparcos instrument.

This chapter provides a relatively complete documentation of the geometrical instrument parameters as determined by the FAST and NDAC consortia. The main results are given in the form of diagrams showing the temporal evolution of each parameter over the whole mission. Since the consortia used different models for the field distortions, different sets of parameters were used and their intercomparison is not always a simple matter (see also Section 9.8). Section 10.2 gives the approximate relations between the two sets of parameters, but the two representations are not strictly comparable, because of the different procedures and conventions adopted. In particular it should be noted that the grid coordinate, as defined by FAST, was obtained from a weighted mean of the phases of the first and second harmonics of the image dissector tube signal, while in NDAC only the first harmonic was used. The phase difference between the harmonics was a function both of time and position in the fields, as illustrated in Figures 5.5 and 5.6.

The geometrical instrument parameters are here presented without any discussion of the actual values and their evolution. An attempt at a physical interpretation of some of the FAST and NDAC instrument parameters is however made in Volume 2, Chapter 10.

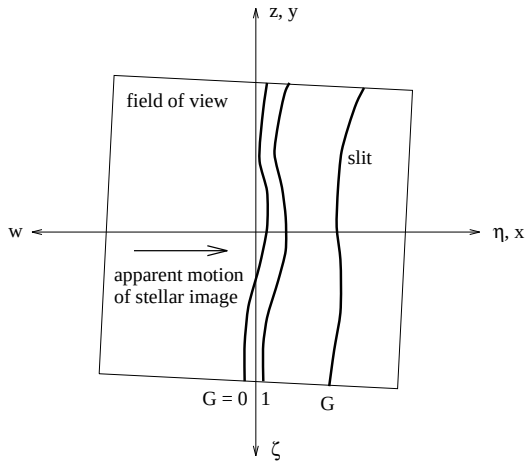

Figure 10.1. *Definition of the grid coordinate G (= number of slits, reckoned from a conventional point near the grid centre) and the approximate orientations of the axes for the field angles* (η, ζ)*, the FAST field coordinates* (x, y)*, and the NDAC field coordinates* (w, z)*. The sense of* $+\eta$*,* $+x$ *and* $-w$ *is given by the apparent motion of stellar images in the field; the perpendicular axes are directed such that the image of the Sun would be in the hemisphere* $-\zeta$*,* $+y$ *or* $+z$*.*

The instrument parameters represent the large-scale part of the transformation from field angles to grid coordinates. A complete description of the grid pattern requires also a medium- and a small-scale component. The medium-scale component is discussed in Section 10.3. The small-scale component was, in the data analysis, treated as noise.

10.2. Geometrical Instrument Parameters

The light modulation produced by the grid allowed the instants when the star image was exactly centred on one of the 2688 slits of the main grid to be determined. The term 'centred' can be loosely understood as meaning 'maximum intensity', but the precise meaning depends on the fitting of a Fourier model of the intensity variations (Section 5.2) and the subsequent definition of the 'reference phase', which, as already mentioned, differed slightly between FAST and NDAC. In practice this led to differences of the order of 10 mas between the two representations; these differences are not further considered here. Conceptually, therefore, the only directly observable 'coordinate' was a quantity G which may be defined as $G = 0$ at the designated central slit, and incrementing by one unit for each slit in the direction of the motion of the stellar image (Figure 10.1). This continuous grid coordinate was related to the true angles as projected on the sky, or the field coordinates, by means of the so-called field-to-grid transformation. (The FAST grid coordinate G in Section 5.4 is similar to the G defined here, only multiplied by the nominal grid period.)

Field Coordinates

Inevitably NDAC and FAST chose different conventions for expressing the angular coordinates in the field. Both may be defined in terms of a third set of field coordinates, the so-called field angles (η, ζ). The field angles are spherical coordinates with $\zeta = 0$ representing the viewing plane through the two sky projections of the star mapper apex and with $\eta = 0$ at the geometrical centre of the grid, i.e. halfway between the 1344th

and 1345th slits, as reckoned from the edge of the main grid where the stellar images entered.

The FAST field coordinates (x, y) are similar to (η, ζ) except that the y axis is in the opposite direction and the origin is taken to be at the 1344th slit; thus:

$$\begin{aligned} x &= \eta + \tfrac{1}{2}s \\ y &= -\zeta \end{aligned} \qquad [10.1]$$

where $s \simeq 1.208$ arcsec is the grid period. The NDAC field coordinates (w, z) are the direction cosines:

$$\begin{aligned} w &= -\cos\zeta \sin\eta \\ z &= -\sin\zeta \end{aligned} \qquad [10.2]$$

The transformation from FAST to NDAC coordinates is, therefore:

$$\begin{aligned} x &= -\arcsin\frac{w}{\sqrt{1-z^2}} + \tfrac{1}{2}s \\ y &= \arcsin z \end{aligned} \qquad [10.3]$$

with the reverse transformation:

$$\begin{aligned} w &= -\cos y \sin(x - \tfrac{1}{2}s) \\ z &= \sin y \end{aligned} \qquad [10.4]$$

The shift by a half grid step between the NDAC and FAST origins is of no consequence for the presentation of the instrument parameters, and the term $\frac{1}{2}s$ is subsequently dropped.

Field-to-Grid Transformation

The complete field-to-grid transformation can be written in the form:

$$G = G_{\text{ref}}(\eta, \zeta) + \Delta G(\eta, \zeta, f, C, t) + \delta G(\eta, \zeta) + \delta g \qquad [10.5]$$

where G_{ref} is a fixed reference model for the field-to-grid transformation, ΔG is the large-scale distortion relative to the reference model, δG the medium-scale distortion and δg the small-scale distortion. (η, ζ) was replaced by (x, y) and (w, z) in the detailed representations of FAST and NDAC. The large-scale distortion was given by a polynomial model and included terms depending on the field index ($f = +1$ for the preceding field of view and $f = -1$ for the following field of view), the colour parameter $C = (B - V) - 0.5$ or $(V - I) - 0.5$, and time.

The time dependence was usually taken care of by the independent solution of the instrument parameters for each reference great circle, i.e. about twice per day. In the FAST reductions of some great circles explicit time-dependent terms were included. In the final iteration this concerned 57 great circles. The results in a few cases where the basic angle showed significant variation are given in Volume 2, Section 12.4.

The medium-scale distortion was generally a fixed matrix of corrections which was derived either empirically, by mapping the residuals of many great-circle reductions, or from laboratory measurements of the grid (Section 10.3). The small-scale distortion described the irregularities of the individual slits and was treated as noise in the data reductions.

Reference Model

The reference model differed between the consortia. $G_{\rm ref}$ was in NDAC taken to be the nominal field-to-grid transformation for the nominal values of the grid step (s_0 = 1.208 arcsec exactly) and basic angle ($\gamma_0 = 58^\circ\,00'\,30''$ exactly). Since the slits were nominally parallel and equidistant in an orthographic projection onto the tangent plane of the curved grid, the nominal relation was:

$$G_{\rm ref\ N} = -S_0 w \qquad [10.6]$$

where S_0 = 170 749.01 slits/rad is the nominal scale corresponding to a grid step of exactly 1.208 arcsec. FAST adopted the same nominal scale at the grid centre, but defined the reference grid coordinate to be proportional to the angle x rather than to the direction cosine w:

$$G_{\rm ref\ F} = S_0 x \qquad [10.7]$$

As a consequence the FAST large-scale distortion contained components attributable to the nominal grid pattern. These components can be derived from Equation 10.4 by means of a series expansion of the trigonometric functions. Since $|x|, |y| < 0.01$, terms of order $O(x^5)$ are smaller than 0.02 mas and can be neglected; hence:

$$G_{\rm ref\ N} = G_{\rm ref\ F} - \tfrac{1}{6} S_0 x^3 - \tfrac{1}{2} S_0 x y^2 \qquad [10.8]$$

Large-Scale Distortion Models

Both consortia used polynomials in the field coordinates to model the large-scale distortion ΔG in Equation 10.5. This choice was motivated by optical calculations, showing that perturbations of the nominal instrument produced distortions which were accurately represented by low-order polynomials (e.g. Bertani *et al.* 1986).

The polynomials were expressed in terms of the normalized field coordinates $\bar{w} = w/q$, $\bar{z} = z/q$, $\bar{x} = x/q$, $\bar{y} = y/q$, where $q = \sin 0\overset{\circ}{.}45$ or $q = 0\overset{\circ}{.}45$, respectively, is the approximate extension of the field of view in either direction from the origin. The quantity q, regarded as a unit for the field coordinates, is also denoted 'hfov' (half field-of-view). The polynomial coefficients thus give the distortion produced by the term at the corner of the field of view (i.e. $\bar{w} = \bar{z} = 1$), and are conveniently expressed in mas/hfov^n, where n is the degree of the distortion term.

The NDAC representation of the large-scale distortion was:

$$G = G_{\rm ref\ N} + s^{-1} \sum_{\substack{0\le i \\ 0\le j \\ 0\le i+j\le 4}} (g_{ij} \pm h_{ij}) \bar{w}^i \bar{z}^j + s^{-1} \sum_{\substack{0\le i \\ 0\le j \\ 0\le i+j\le 1}} (c_{ij} \pm d_{ij}) \bar{w}^i \bar{z}^j C \qquad [10.9]$$

where, in the final reductions, $C = (V - I) - 0.5$. Upper and lower signs refer to the preceding ($f = +1$) and following ($f = -1$) field of view, respectively. The factor s^{-1} takes into account that the sums give the distortion in angular measure (e.g. milliarcsec), while G is measured in grid steps. In Equation 10.9 the terms containing g_{00} and c_{00} were excluded because they cannot be estimated in the great-circle reductions. g_{00} represents the origin of the field coordinate w and was set to zero by definition. c_{00} represents the so-called 'constant chromaticity' that was instead estimated in the sphere solution (see Section 16.3). The model thus contained 34 instrument parameters. The quartic

terms ($i + j = 4$) were partially kept constant and are not discussed in the following. The temporal evolution of the remaining 24 parameters are shown in Figures 10.2 to 10.7.

The FAST representation may be written:

$$G = G_{\text{ref F}} - s^{-1}\sum_{\substack{0\le i\\0\le j\\1\le i+j\le 4}} a_{ij}^{\text{p/f}}\,\bar{x}^i\,\bar{y}^j - s^{-1}\sum_{\substack{0\le i\\0\le j\\i+j=1}} b_{ij}^{\text{p/f}}\,\bar{x}^i\,\bar{y}^j C \pm \tfrac{1}{2}s^{-1}(\Delta\gamma_0 + \Delta\gamma_1 C) \qquad [10.10]$$

where, again, $C = (V - I) - 0.5$ and the upper/lower sign refers to the preceding/following field of view. For the field distortion, a separate set of coefficients is used in each field of view, namely a_{ij}^{p} and b_{ij}^{p} in the preceding field, a_{ij}^{f} and b_{ij}^{f} in the following. $\Delta\gamma_0$ is the correction to the reference value of the basic angle; $\Delta\gamma_1$ is the chromatic variation of the basic angle. The total number of parameters is 34, of which the first 24 are displayed in Figures 10.8 to 10.13. The cubic and quartic terms were fixed at their values determined in earlier iterations, and the quartic terms are not displayed. In some great-circle reductions, considered too short to give better estimates, some of the lower-order parameters were also fixed (see Section 9.6).

Relations Between the NDAC and FAST Instrument Parameters

As previously mentioned, no strict relation exists between the NDAC and FAST instrument parameters due to the different treatments of the signal harmonics. Disregarding this difficulty, the approximate relations can be established by equating the G in Equations 10.9 and 10.10. Using Equation 10.8 and, in the polynomials, the approximations $\bar{w} \simeq -\bar{x}$ and $\bar{z} \simeq \bar{y}$, the relations become:

$$a_{ij}^{\text{p/f}} = (-1)^{i+1}(g_{ij} \pm h_{ij}) + \begin{cases} \frac{1}{6}S_0 sq^3 & \text{if } (i,j) = (3,0) \\ \frac{1}{2}S_0 sq^3 & \text{if } (i,j) = (1,2) \\ 0 & \text{otherwise} \end{cases} \qquad [10.11]$$

The additional terms for $(i, j) = (3, 0)$ and $(1, 2)$ represent the nominal distortion of the grid and amount to 16.65 mas/hfov^3 and 49.96 mas/hfov^3, respectively. Relations analogous to Equation 10.11 are found among the chromatic terms. For the zero-order terms the relations $\Delta\gamma_0 = 2h_{00}$ and $\Delta\gamma_1 = 2d_{00}$ are found. Table 10.1 provides the explicit relations for all the parameters displayed in Figures 10.2 to 10.13. Results of an actual comparison for a particular great circle are shown in Figures 9.15 and 9.16.

10.3. Medium-Scale Distortion

The medium-scale distortion, represented in Equation 10.5 by the term $\delta G(\eta, \zeta)$, was in the FAST reductions applied as *a priori* corrections $\delta p = s\delta G$ to the relative modulation phases of the image dissector tube samples for each interlacing period ($T_3 = 0.133\ldots$ s), as described in Section 5.4. Thus, this term was in principle eliminated before the great-circle reductions and should not appear in the FAST field-to-grid transformation. The corrections were derived from the laboratory measurements displayed in the lower-left panel of Figure 10.15. The measurements gave a mean displacement for each scan field, thus providing a correction matrix of 168×46 values for the whole main grid.

In the NDAC reductions, the modulation phases were not corrected by the laboratory measurements. Instead, the residuals of the great-circle reductions (one per star and

observation frame of $T_4 = 2.133\ldots$ s) were accumulated in maps of 18×46 areas covering each field of view. The resolution in the scanning direction of $0\overset{\circ}{.}9/18 = 0\overset{\circ}{.}05$ corresponded to the motion of stellar images in half an observational frame and thus provided a sufficient oversampling of the irregularities smeared by the distribution of samples in the observational frame. The binning of residuals in the perpendicular direction coincided with the division into scan fields.

Residual maps were calculated for the preceding and following fields and separately for each great-circle reduction, and later averaged over longer periods of time. Figures 10.14 and 10.15 show the mean residuals from the provisional processing of the first year of satellite data. Each pair of maps represents some three to five months of observations. The pattern of residuals is remarkably stable, and also fairly similar in the two fields of view, indicating that much of the details are due to the irregularities of the grid. This is also supported by a comparison with the laboratory measurements, after convolution with the observational frame and subtraction of a fourth-degree polynomial (Figure 10.15, lower-right panel). Although the overall resemblance to the residual maps is not striking, there are many detailed similarities validating the laboratory measurements. The residual and laboratory maps are also compared, after averaging in the z direction, in Figure 10.16. Although the laboratory measurements were smeared by the width of the observational frame, their amplitude appears to be substantially larger than the variations of the residuals. This could indicate that an additional smearing mechanism was at work in the great-circle reductions, or that the medium-scale distortions at frame level were underestimated by the mapping process.

After the provisional processing of the first year of data, the resulting mean residual maps were adopted as fixed corrections to the grid coordinates taken as input to the great-circle reductions. These corrections were applied to all the subsequent great-circle reductions in NDAC, including the reprocessing of the first year of data.

L. Lindegren, H. Schrijver, F. van Leeuwen

Table 10.1. Approximate relations between the FAST and NDAC instrument parameters.

FAST parameters in terms of NDAC parameters		Unit	Meaning
$\Delta\gamma_0 = \ 2h_{00}$		mas	basic angle
$a^{\mathrm{p}}_{10} = \ g_{10} + h_{10}$	$a^{\mathrm{f}}_{10} = \ g_{10} - h_{10}$	mas/hfov	scale
$a^{\mathrm{p}}_{01} = -g_{01} - h_{01}$	$a^{\mathrm{f}}_{01} = -g_{01} + h_{01}$	mas/hfov	rotation
$a^{\mathrm{p}}_{20} = -g_{20} - h_{20}$	$a^{\mathrm{f}}_{20} = -g_{20} + h_{20}$	mas/hfov^2	tilt
$a^{\mathrm{p}}_{11} = \ g_{11} + h_{11}$	$a^{\mathrm{f}}_{11} = \ g_{11} - h_{11}$	mas/hfov^2	„
$a^{\mathrm{p}}_{02} = -g_{02} - h_{02}$	$a^{\mathrm{f}}_{02} = -g_{02} + h_{02}$	mas/hfov^2	„
$a^{\mathrm{p}}_{30} = \ g_{30} + h_{30} + 16.65$	$a^{\mathrm{f}}_{30} = \ g_{30} - h_{30} + 16.65$	mas/hfov^3	cubic distortion
$a^{\mathrm{p}}_{21} = -g_{21} - h_{21}$	$a^{\mathrm{f}}_{21} = -g_{21} + h_{21}$	mas/hfov^3	(including nominal)
$a^{\mathrm{p}}_{12} = \ g_{12} + h_{12} + 49.96$	$a^{\mathrm{f}}_{12} = \ g_{12} - h_{12} + 49.96$	mas/hfov^3	„
$a^{\mathrm{p}}_{03} = -g_{03} - h_{03}$	$a^{\mathrm{f}}_{03} = -g_{03} + h_{03}$	mas/hfov^3	„
$\Delta\gamma_1 = \ 2d_{00}$		mas/mag	chrom. basic angle
$b^{\mathrm{p}}_{10} = \ c_{10} + d_{10}$	$b^{\mathrm{f}}_{10} = \ c_{10} - d_{10}$	mas/hfov/mag	chrom. scale
$b^{\mathrm{p}}_{01} = -c_{01} - d_{01}$	$b^{\mathrm{f}}_{01} = -c_{01} + d_{01}$	mas/hfov/mag	chrom. rotation

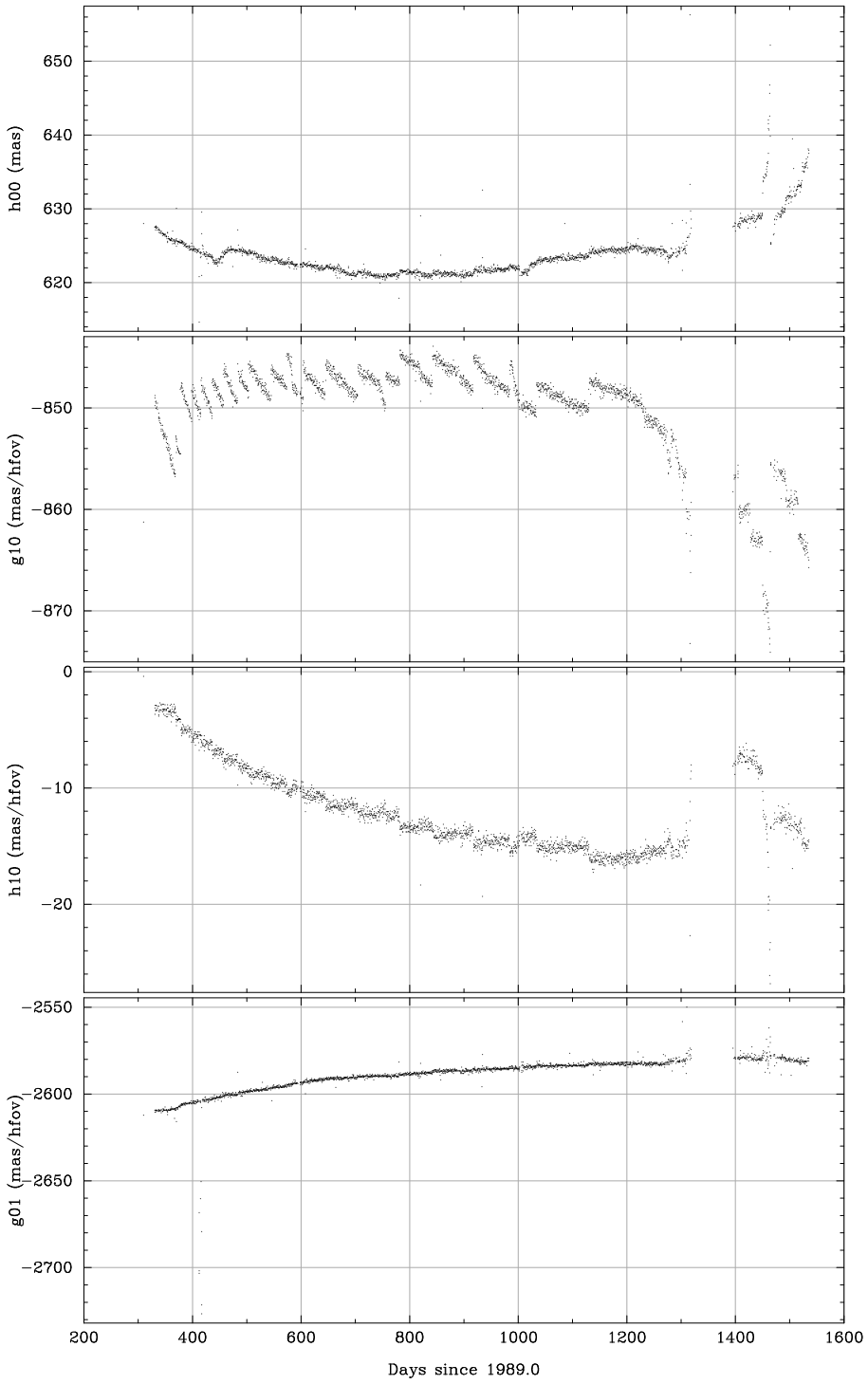

Figure 10.2. *Evolution of the NDAC instrument parameters* h_{00}, g_{10}, h_{10} *and* g_{01}.

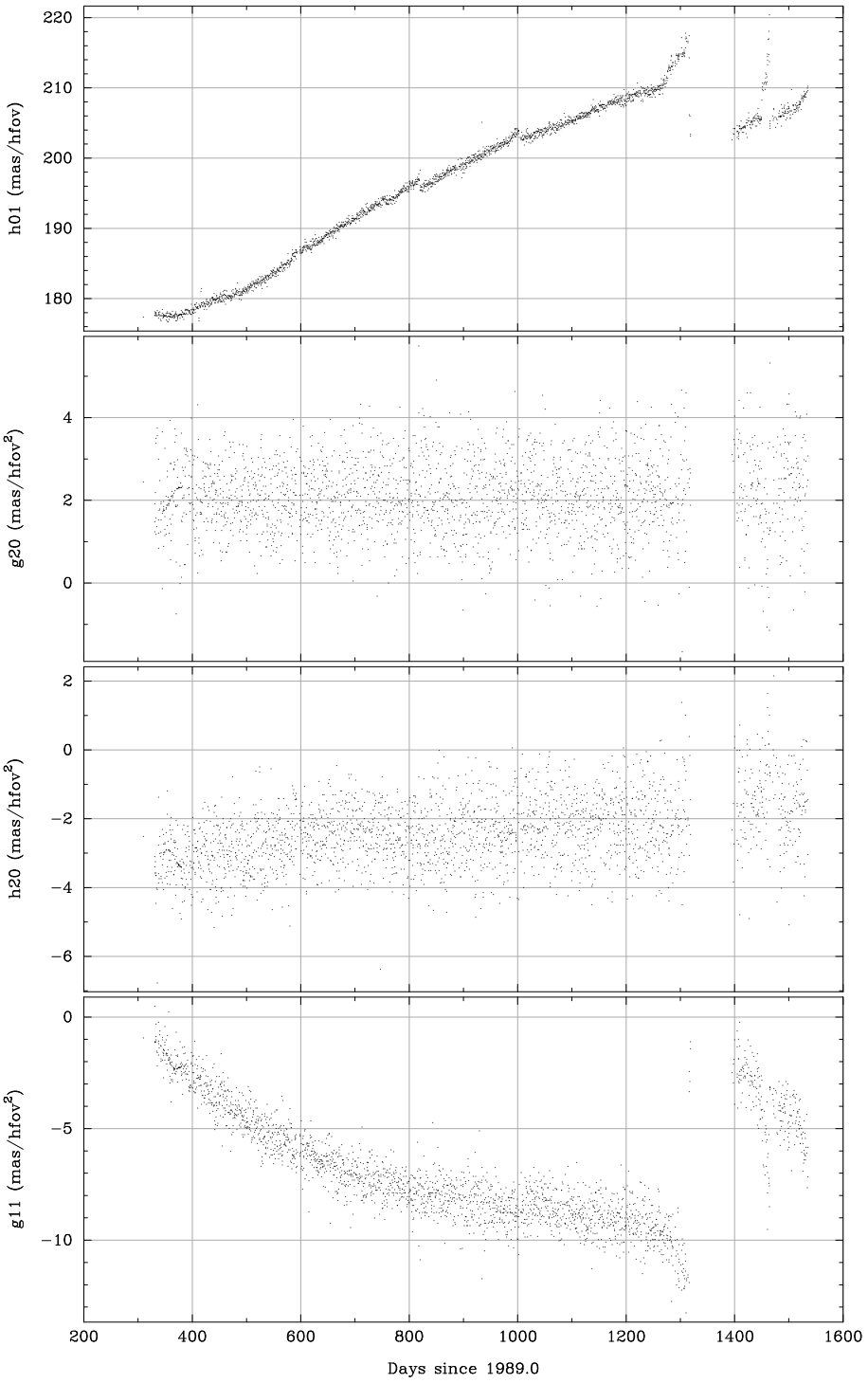

Figure 10.3. *Evolution of the NDAC instrument parameters* h_{01}, g_{20}, h_{20} *and* g_{11}.

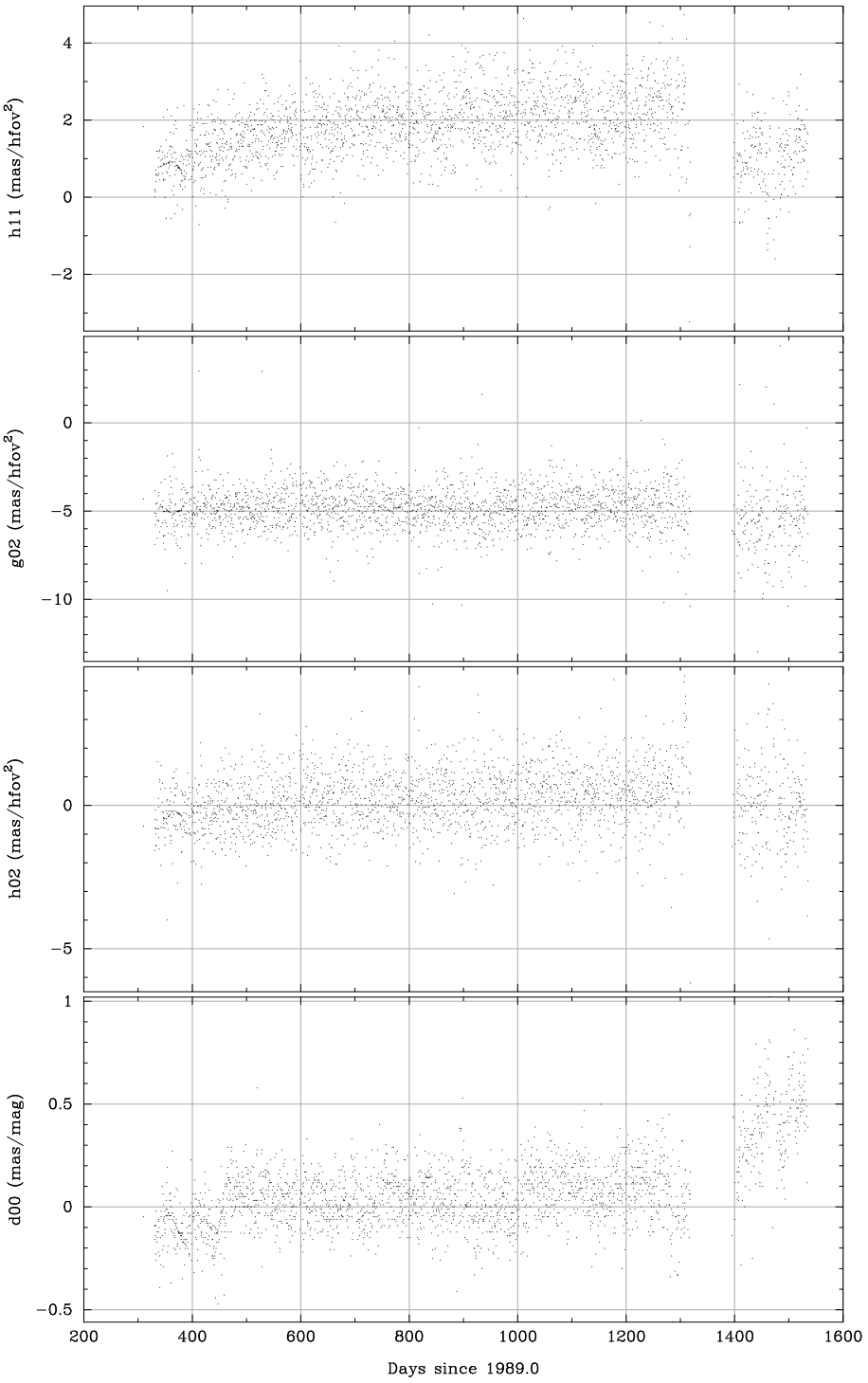

Figure 10.4. *Evolution of the NDAC instrument parameters* h_{11}, g_{02}, h_{02} *and* d_{00}.

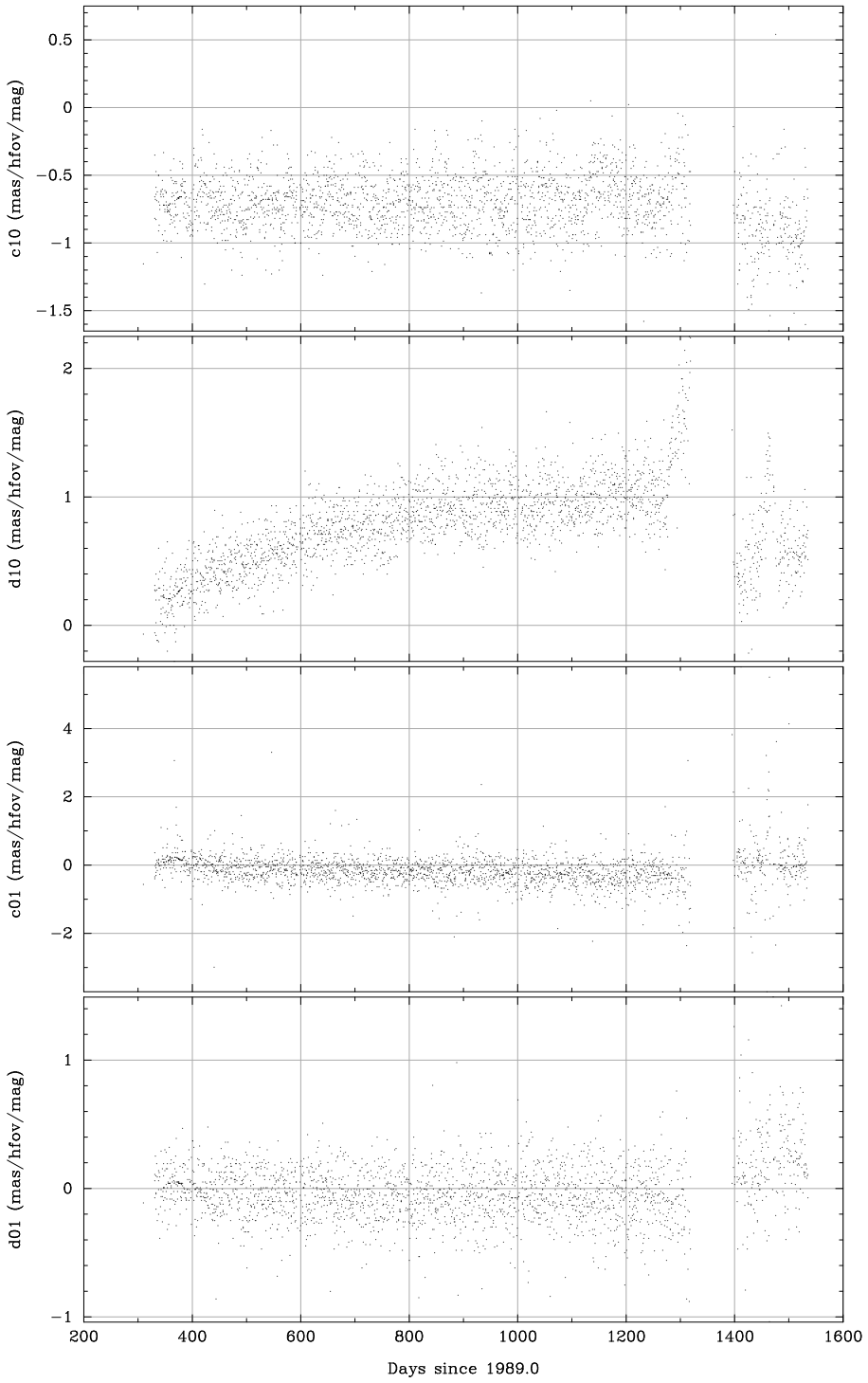

Figure 10.5. *Evolution of the NDAC instrument parameters* c_{10}, d_{10}, c_{01} *and* d_{01}.

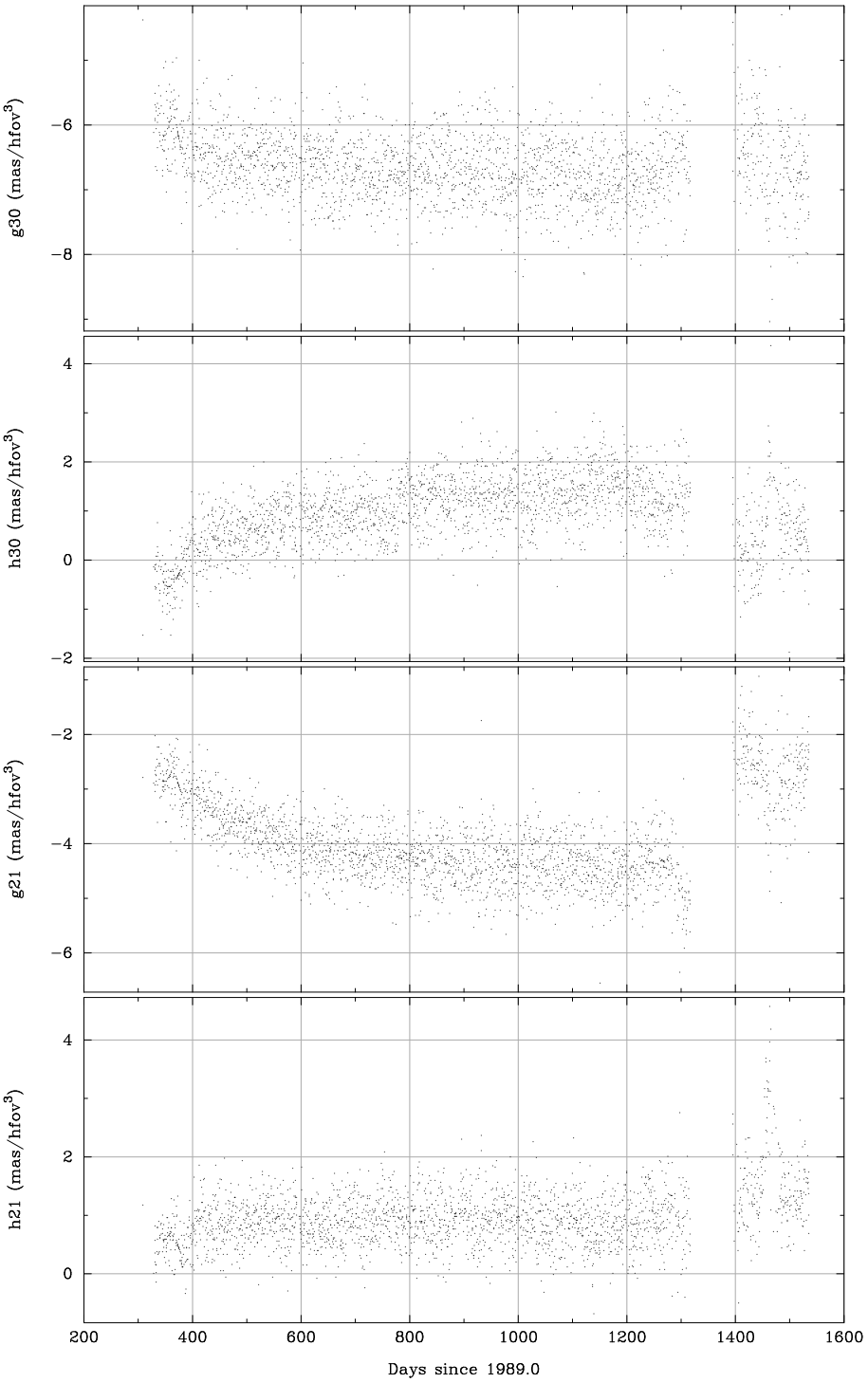

Figure 10.6. *Evolution of the NDAC instrument parameters* g_{30}, h_{30}, g_{21} *and* h_{21}.

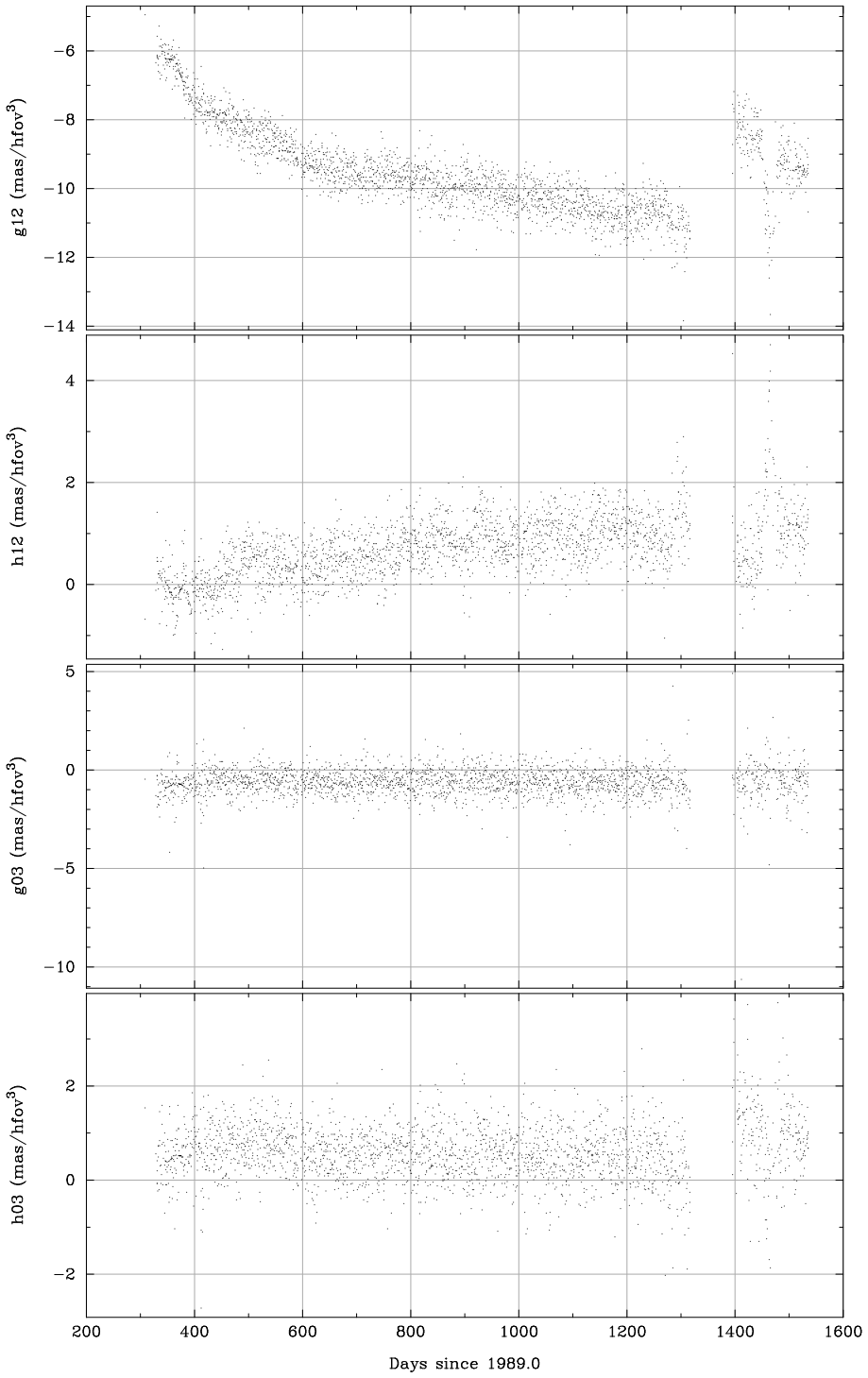

Figure 10.7. *Evolution of the NDAC instrument parameters* g_{12}, h_{12}, g_{03} *and* h_{03}.

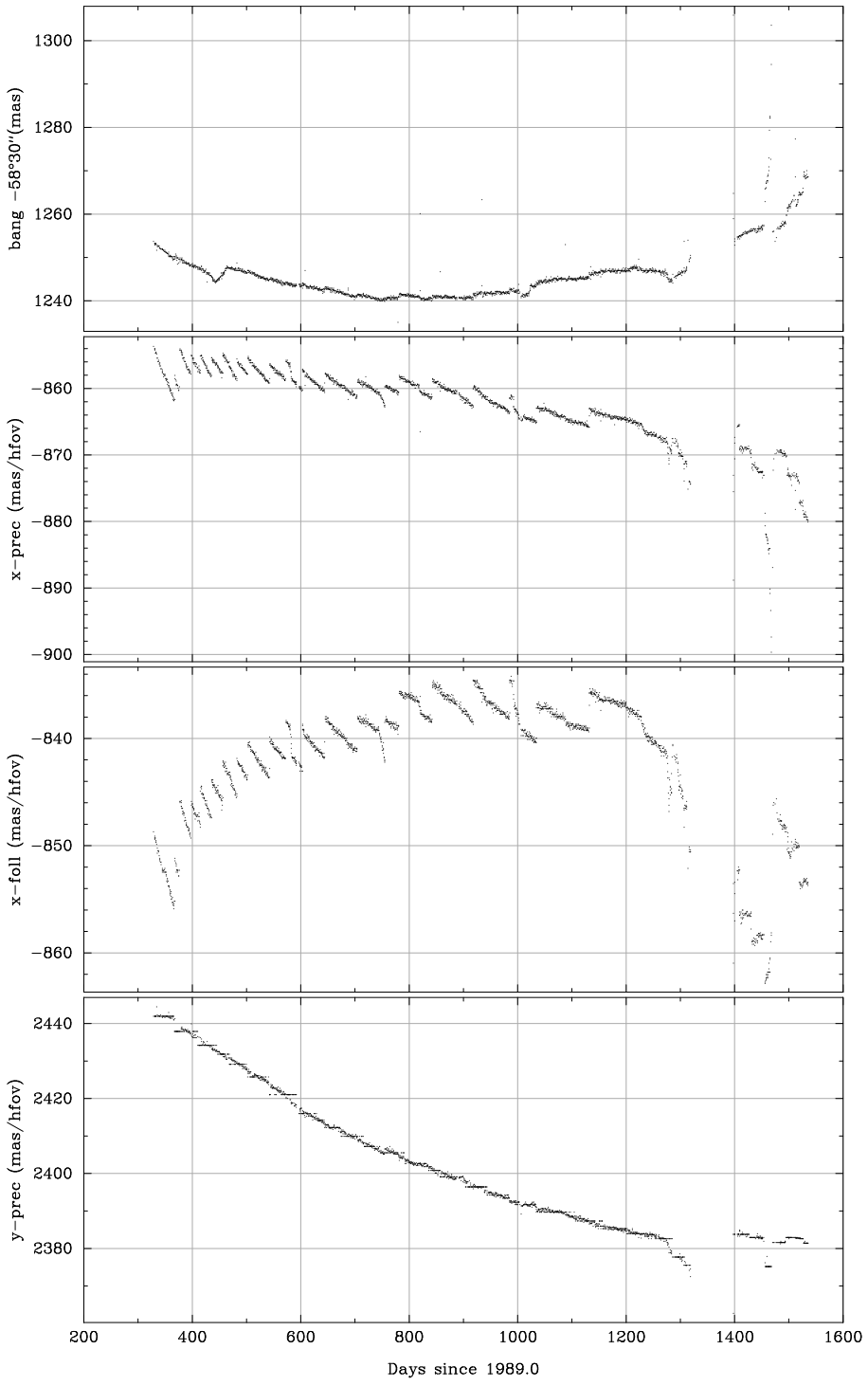

Figure 10.8. *Evolution of the FAST instrument parameters* $\Delta\gamma_0$ *[bang],* a_{10}^{p} *[x-prec],* a_{10}^{f} *[x-foll],* a_{01}^{p} *[y-prec].*

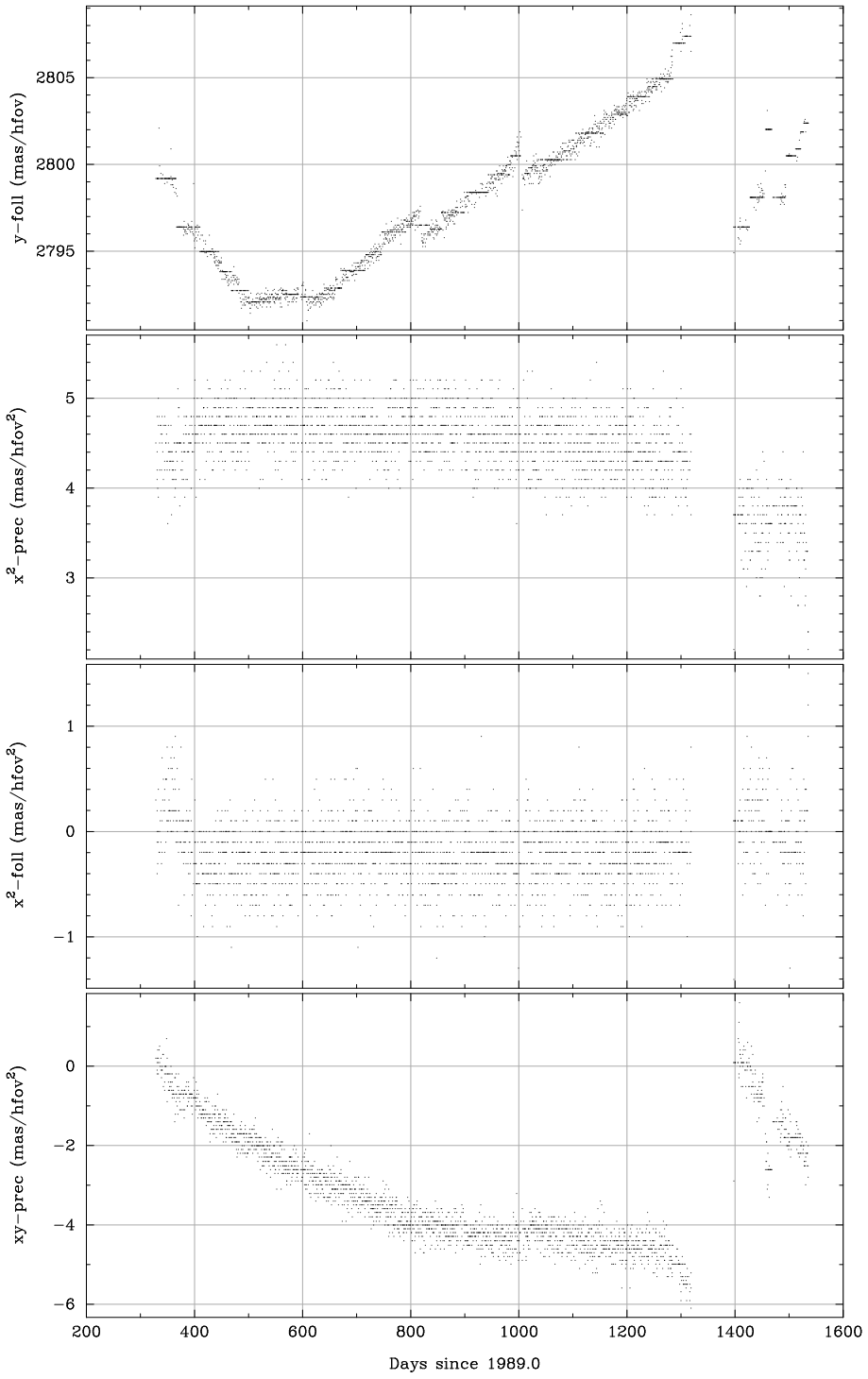

Figure 10.9. *Evolution of the FAST instrument parameters* a^{f}_{01} *[y-foll],* a^{p}_{20} *[x^2-prec],* a^{f}_{20} *[x^2-foll] and* a^{p}_{11} *[xy-prec].*

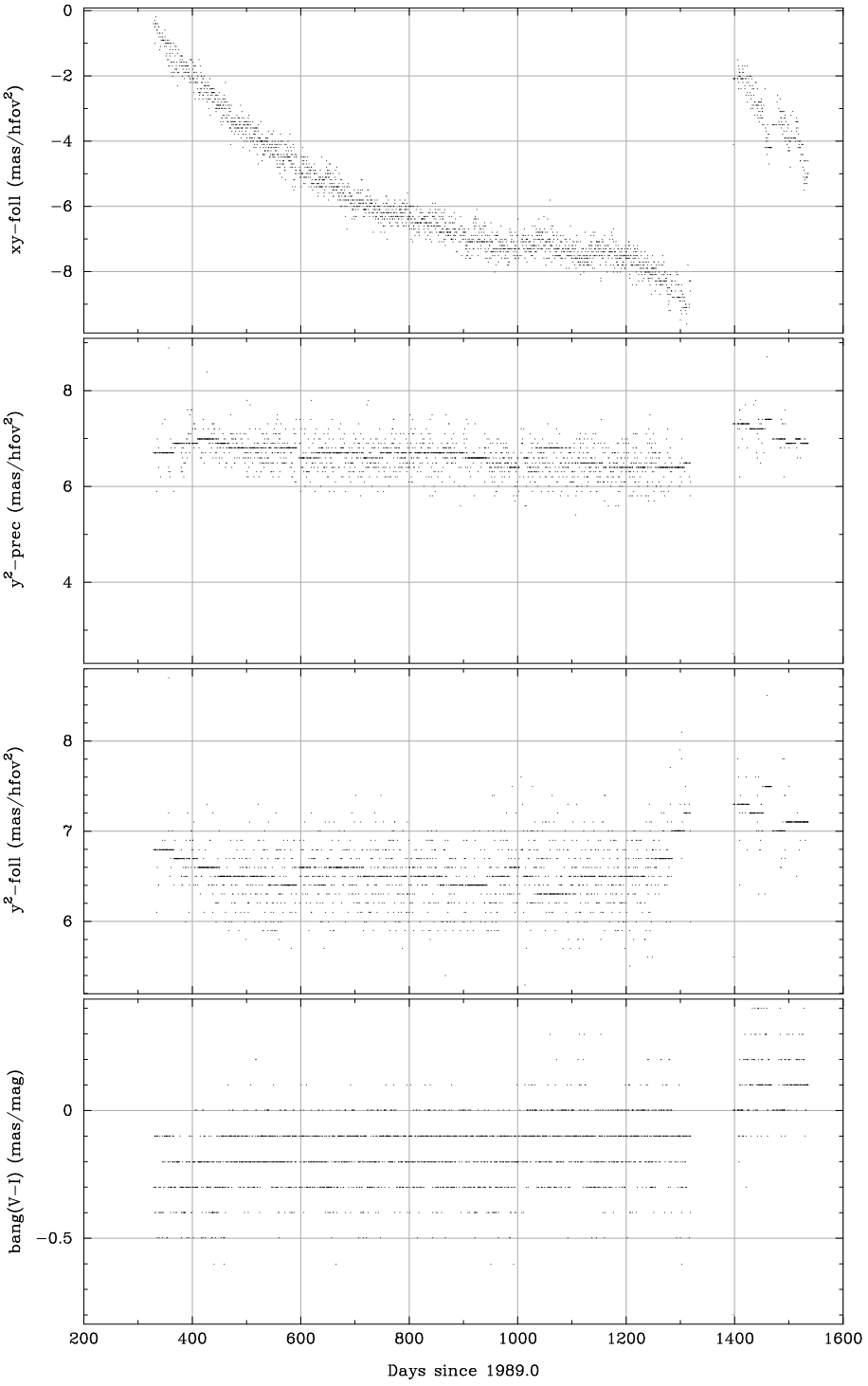

Figure 10.10. *Evolution of the FAST instrument parameters* a_{11}^{f} *[xy-foll],* a_{02}^{p} *[y^2-prec],* a_{02}^{f} *[y^2-foll] and* $\Delta\gamma_1$ *[bang(V-I)].*

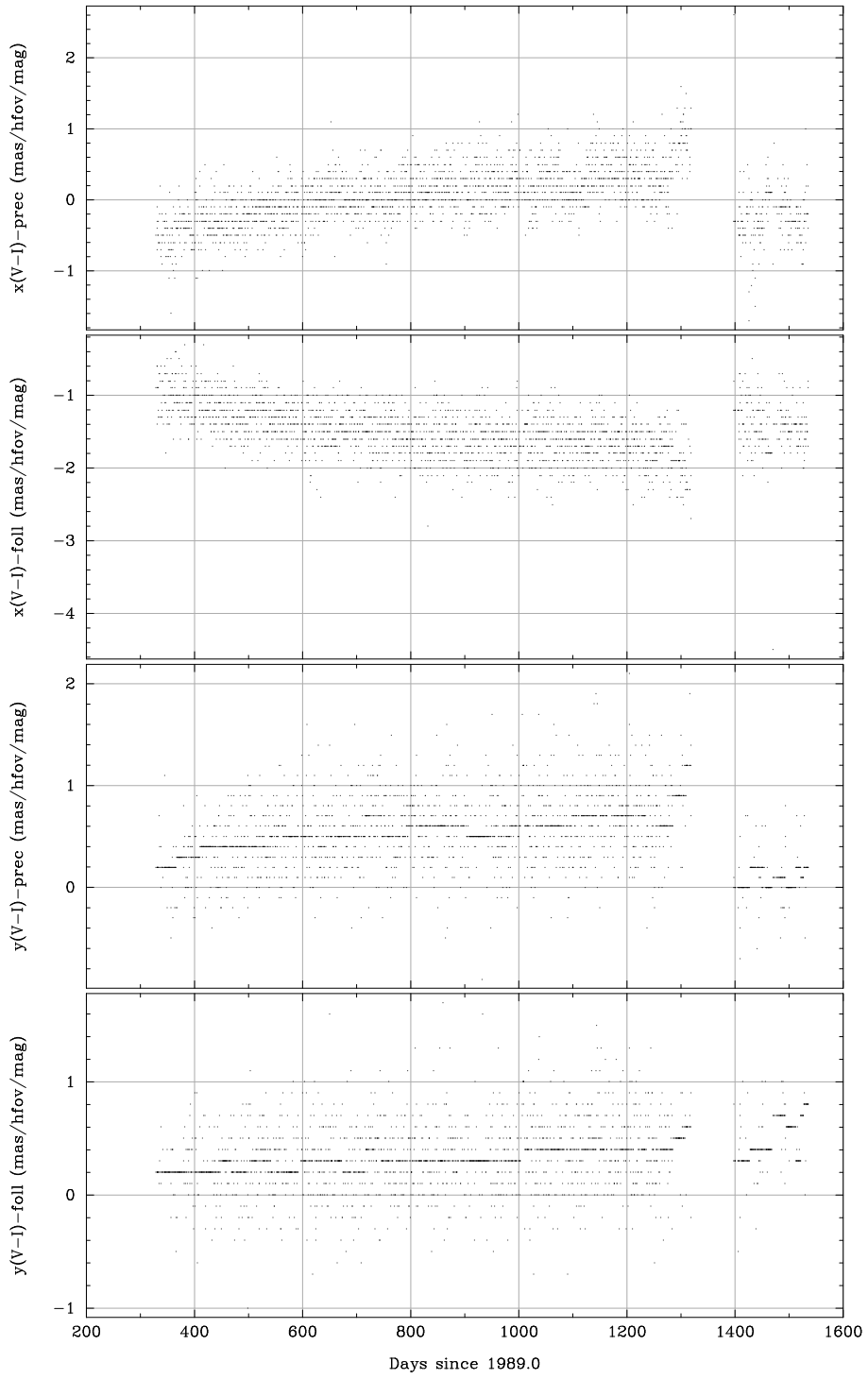

Figure 10.11. *Evolution of the FAST instrument parameters* b^{p}_{10} *[x(V-I)-prec],* b^{f}_{10} *[x(V-I)-foll],* b^{p}_{01} *[y(V-I)-prec] and* b^{f}_{01} *[y(V-I)-foll].*

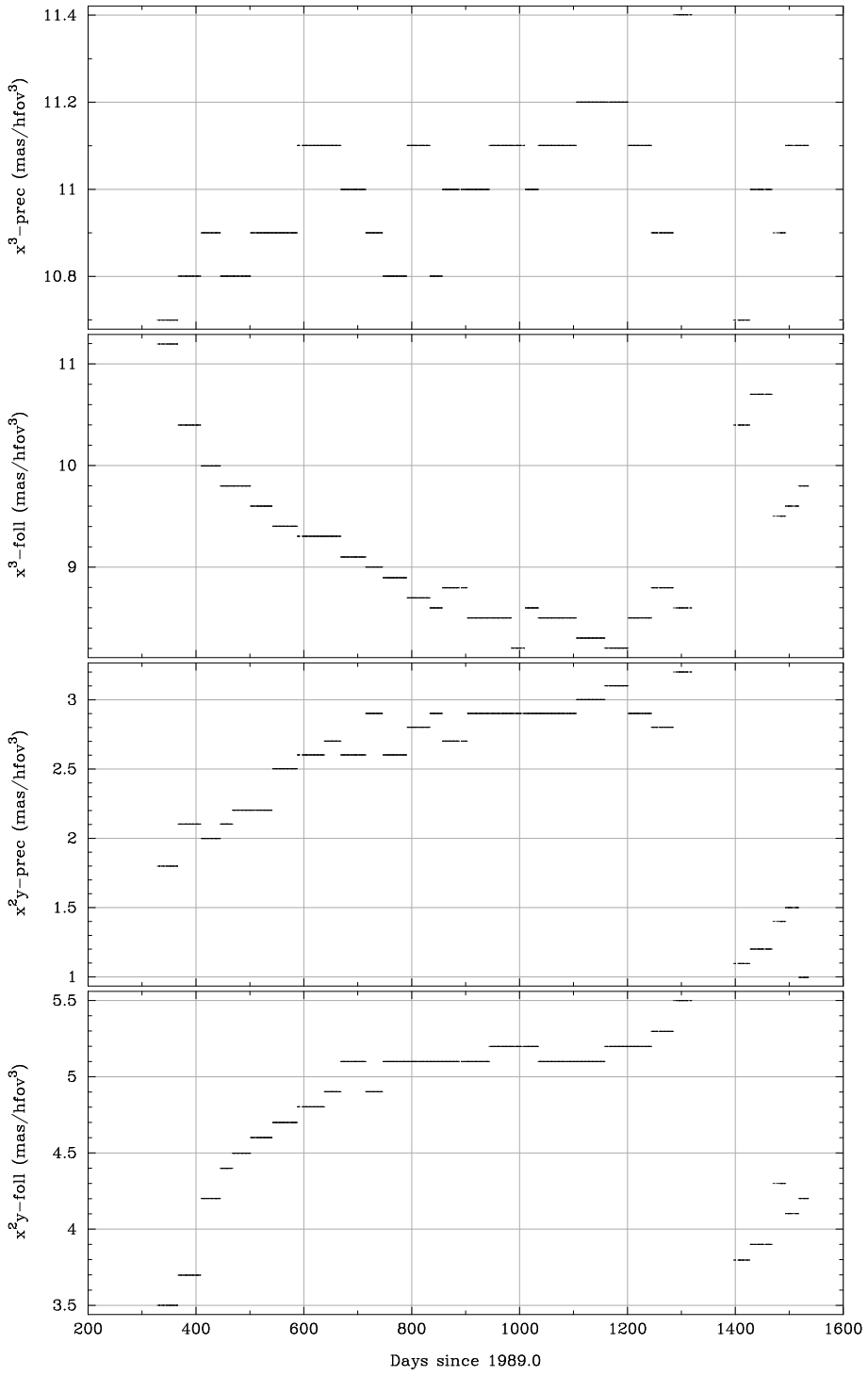

Figure 10.12. *Evolution of the FAST instrument parameters* a_{30}^{p} *[*x^3*-prec],* a_{30}^{f} *[*x^3*-foll],* a_{21}^{p} *[*x^2y*-prec] and* a_{21}^{f} *[*x^2y*-foll].*

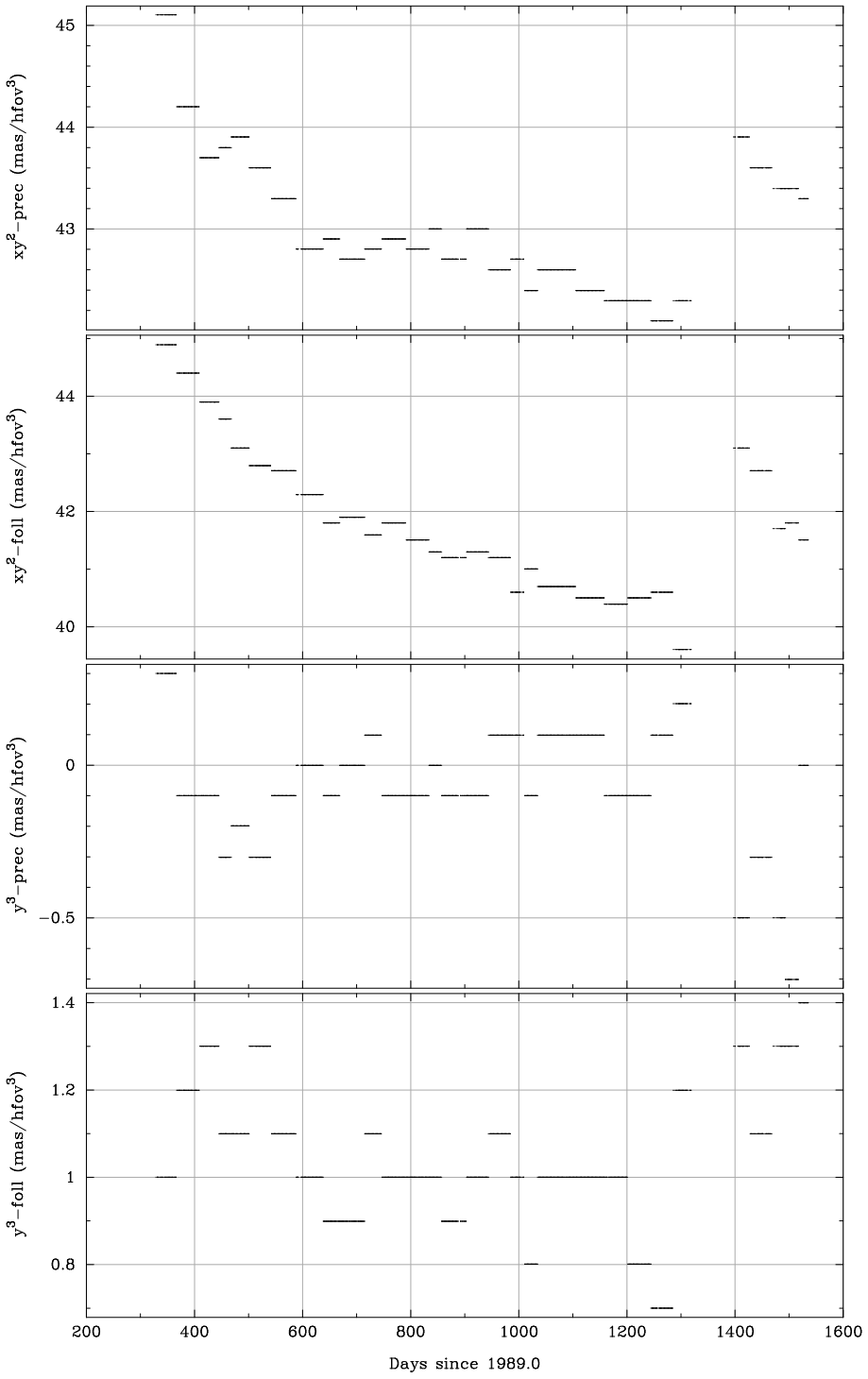

Figure 10.13. *Evolution of the FAST instrument parameters* a_{12}^{p} *[xy²-prec],* a_{12}^{f} *[xy²-foll],* a_{03}^{p} *[y³-prec] and* a_{03}^{f} *[y³-foll].*

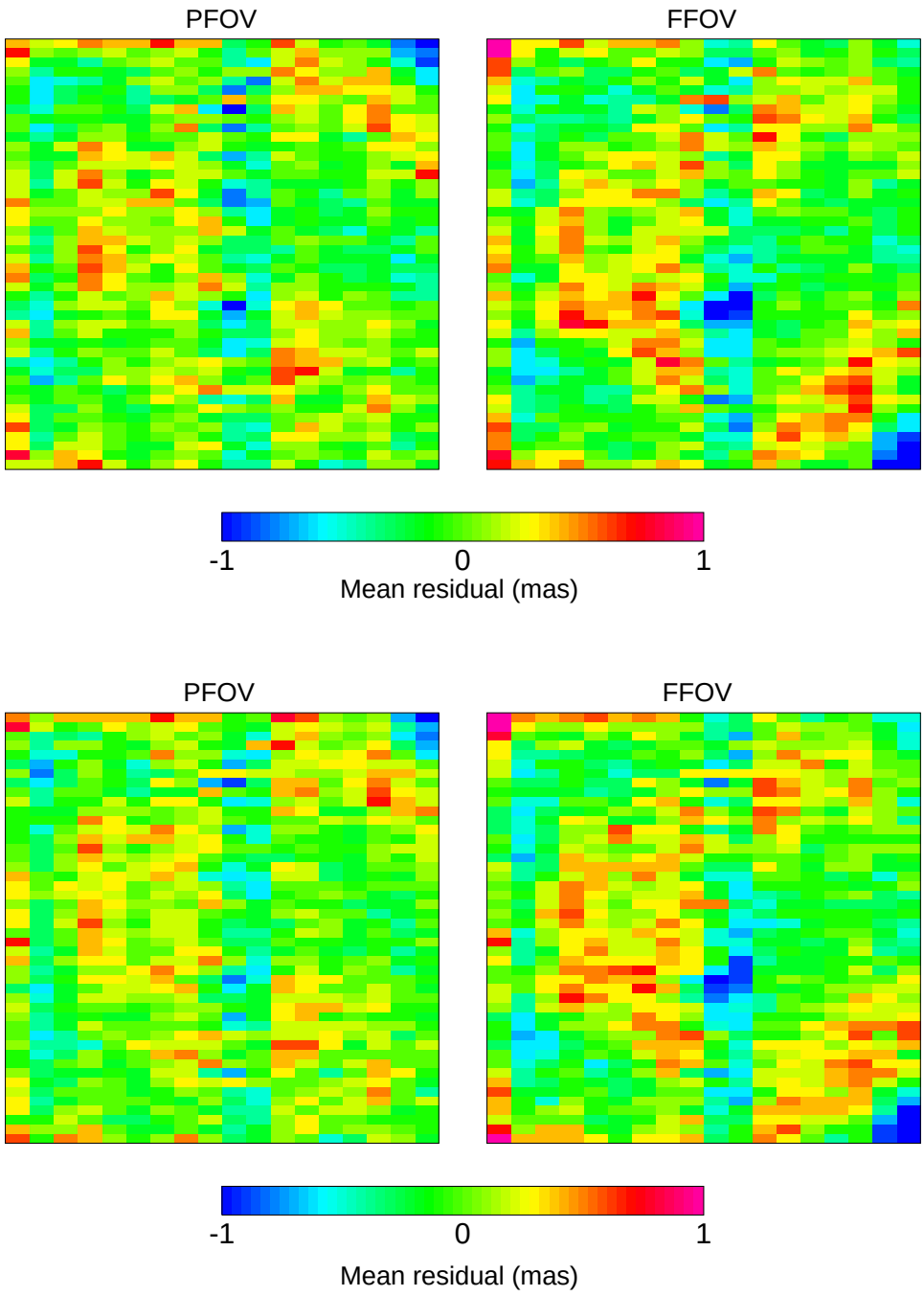

Figure 10.14. *Maps of the mean residuals of the provisional NDAC great-circle reductions for the first year of data. The mean values of* $G_{\rm obs} - G_{\rm calc}$ *are shown as function of the position in the preceding field of view (PFOV, to the left) and following field of view (FFOV, to the right). The area reproduced corresponds exactly to the area of the main grid* ($0\overset{\circ}{.}9 \times 0\overset{\circ}{.}9$)*. The orientation of the maps is the same as in Figure 10.1, and is such that the rotation of the satellite caused star images to move from left to right, and the image of the Sun would be far up in the maps. The two upper maps are for orbits 1 to 415, the two lower maps are for orbits 416 to 685.*

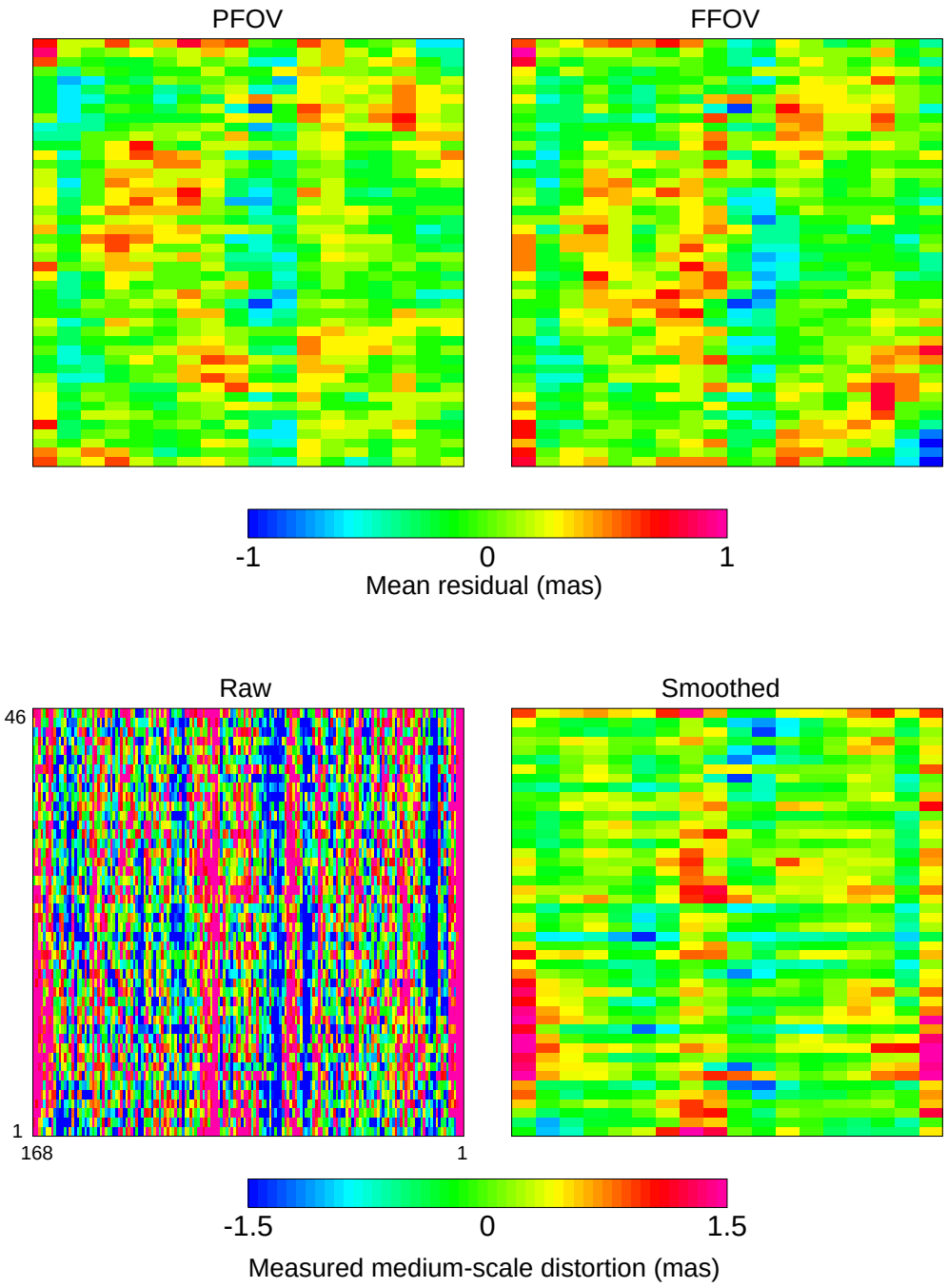

Figure 10.15. *The two upper maps show the mean residuals of the provisional NDAC great-circle reductions for orbits 686 to 915 in the preceding and following fields of view. The lower maps show the results of laboratory measurements of the medium-scale distortion of the main grid. To the left the measurements of the individual scan fields are displayed; to the right the same data smoothed, in the scanning direction, by a moving average of 6 arcmin width, corresponding to the motion in one observational frame. The scan field indices ($i_G = 1 \ldots 168$, $i_H = 1 \ldots 46$) are indicated next to the lower-left map.*

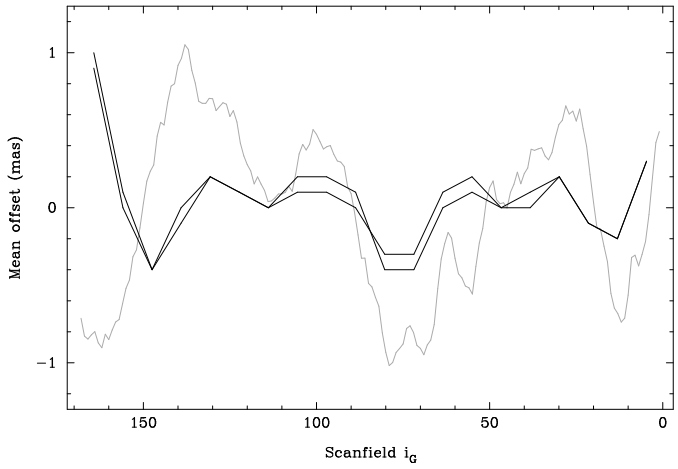

Figure 10.16. *Comparison of the medium-scale distortion derived from the great-circle reductions (solid curves) and the laboratory measurements (dotted curve). This diagram shows the same data as Figures 10.14 and 10.15, but averaged over the z coordinate or scan field index i_H. The two solid curves are for the preceding and following fields. A moving average of 6 arcmin width was applied to the laboratory data in the scanning direction (w or scan field index i_G) to simulate the smearing effect of the observational frame.*